Manufacturing Letters 29 (2021) 5–10

Contents lists available at ScienceDirect

Manufacturing Letters

journal homepage: www.elsevier.com/locate/mfglet

Aerosol jet 3D printing and high temperature characterization of nickel nanoparticle films

Md Taibur Rahman [1], Rahul Panat *

Department of Mechanical Engineering, Carnegie Mellon University, 5000 Forbes Ave, Pittsburgh, PA 15213, USA

ARTICLE INFO

Article history:
Received 2 February 2021
Received in revised form 18 April 2021
Accepted 26 April 2021
Available online 1 May 2021

Keywords:
Nickel nanoparticles
3D printing
Thin films
Oxidation
High-temperature behavior

ABSTRACT

Three-dimensional (3D) nanoparticle printing has emerged as a versatile and environmentally friendly manufacturing technique to fabricate metallic films for microelectronic applications. In this letter, we report the synthesis of 500 nm thick nickel films by aerosol jet nanoparticle printing and assess their stability at high temperatures. In-situ impedance spectroscopy is used to measure the electrical properties of the films from 25 °C to 500 °C, at frequencies from 0.02 kHz to 300 kHz. It is observed that the real part of impedance of the films increases from room temperature to 350 °C monotonously, indicating a positive temperature coefficient of resistance (TCR). Upon further heating, however, the films exhibit an unstable electrical behavior, with TCR increasing by two orders of magnitude between 350 °C and 500 °C. Thermogravimetric analysis (TGA) of nickel nanoparticles was performed to understand the underlying reason of electrical instability beyond 350 °C, which showed that the particle oxidation starts at about 325–350 °C and leads to a mass gain of 19.35% at 500 °C, indicating significant thermal oxidation. The electrical stability of the films at high temperatures is thus controlled by their thermal oxidation, which starts at a much lower temperature (350 °C) when compared to bulk nickel (600 °C). Implications of this result on the applicability of the 3D printing method to synthesize metal films for high temperature applications are discussed.

Additive manufacturing methods have enabled the fabrication of devices with different geometries, microstructures, and material combinations. At micro and nanoscale, additive manufacturing methods such as nanoparticle (NP) printing are allowing the fabrication of films and devices with unique functionalities and applications. Aerosol Jet (AJ) printing is one such method that can rapidly fabricate 3D electronics at a length scale down to 10 μm. In addition, this method creates minimal waste, is low cost, and allows the fabrication of electronic devices on curved surfaces [1,2]. Aerosol jet printing has been used to create devices such as biosensors [3,4], capacitive touch sensors [5], antennas [6], temperature sensors [7], strain sensors [8], flexible interconnects [9], and electronic transistors [10]. In the AJ printing method, the NPs are typically dispersed in a solvent and are dispensed on a substrate, and then sintered using an energy source such as heat [11], laser [12] or photonic flash [13,14].

Several electronic devices are used at high temperatures under harsh environments [7,8,15]. For example, strain and oxygen sensors are used for *in-situ* monitoring of combustion parameters in jet engines to help improve their energy efficiency and safety [16]. The components of the high temperature systems, however, have complex 3-D shapes, making it difficult to fabricate/integrate electronics on their surfaces [17]. Conventional photolithography/MEMS based sensor electronics are limited in their ability to confirm to the 3-D shapes [18] as well as the choices of materials [19] that can survive at high temperatures. Nanoparticle-based additive manufacturing methods can help overcome these challenges with the ability to print various material combinations on curved surfaces. One concern, however, is that oxidation of NPs (in un-sintered format) can happen at temperatures lower than their bulk counterparts due to the high surface-to-volume ratio at the nanoscale [15,20]. Nickel and nickel-based alloys are well-known for corrosion resistance and are used for high temperature applications (e.g., superalloys in jet engine applications). In addition, nickel films are used in electronic components such as multi-layer-ceramic-capacitors, where the films need to withstand high temperatures required for the sintering of ceramic dielectrics [21,22]. Lastly, nickel metal films along with an oxide layer on their surfaces have potential applications in data storage devices [23]. It is thus reasonable to study the synthesis of nickel films using

* Corresponding author.
E-mail address: rpanat@andrew.cmu.edu (R. Panat).
[1] Current address: Technology and Manufacturing Group, Intel Corporation, 5000 W. Chandler Blvd, Chandler AZ 85226 USA.

https://doi.org/10.1016/j.mfglet.2021.04.006
2213-8463/

nanoparticle printing and assess their performance at high temperatures.

Oxidation can cause a significant increase in the impedance of metallic conductors [24]. Unlike bulk materials, however, the nanoparticles oxidize at much lower temperatures [20,25]. This is primarily due to the fact that the high surface-to-volume ratio of the nanoparticles prevents the formation of a stable oxide layer, allowing higher rates of oxidation at lower temperatures compared to the bulk. It is of significant interest to know how *sintered nanoparticle films,* which are typically porous, behave at high temperatures. Such data will greatly aid in opening up of advanced additive manufacturing techniques for high temperature device applications. To date, the oxidation behavior of nickel has been studied via thermogravimetric analysis of nano and microparticles at high temperatures [26–28], with no report for sintered nanoparticle films. Unlike bulk nickel, which starts to oxidize at 700 °C, the oxidation of Ni nanoparticles (10–100 nm in size) occurs at 250 °C [26]. Further, early partial melting of nickel nanoparticles was observed above 600 °C [26], a temperature far below the melting temperature of the bulk (1450 °C). Oxidation of 50 nm thick Ni films was reported to initiate at 400 °C [29].

The impetus for the current work is thus two-fold. First, we aimed to synthesize high quality Ni films using AJ nanoparticle printing, an emerging additive manufacturing method. Second, we desired a fundamental understanding of such films at high temperatures via impedance spectroscopy. The work will open up paths to design and fabricate printed electronics for use at high temperatures and under harsh environments. Electrical properties of AJ printed nickel nanoparticle films are determined in the range of 24–500 °C at frequencies ranging from 0.02 to 300 kHz. Further, scanning electron microcopy (SEM) and thermogravimetric analysis (TGA) are used to correlate the electrical behavior with oxidation of the film which causes its degradation.

An Aerosol Jet 3D printer (AJ-300, Optomec, Inc., Albuquerque, NM) was used to fabricate the Ni NP films in this study. The AJ method allows the deposition of nanoparticles dispersed in a solvent (i.e. nanoparticle ink) onto a substrate by creating a mist of particles guided by a carrier gas. The AJ printing system includes two atomizers (ultrasonic and pneumatic), a programmable XY motion stage (also called platen), and a deposition head. The printing can be done down to feature sizes of about 10 μm with a wide range of ink viscosities up to 1000 cP. The particle size in the inks used in the AJ method is typically < 500 nm and has a printing standoff height of 5 mm [6]. A solvent-based Ni nanoparticle ink (Ni-IJ70, Applied Nanotech, Inc., Austin, Texas) was placed in the atomizer which continuously created the mist droplet size of 1–5 μm (each droplet containing multiple nanoparticles) which was then carried to the deposition head with a carrier gas (N_2) [6]. The nickel nanoparticle size in the ink was 60 ± 40 nm, a solid content of 30 wt% in the ink, and a viscosity of about 16–25 cP according to the manufacturer information. The mist or dense vapor was then focused inside the nozzle with the help of a secondary gas, called sheath gas (also N_2) to form the micro-jet. A transparent glass slide (Thermo-Fisher Scientific, Waltham, MA) was used as the substrate which was placed on the platen heated to 60 °C. See Fig. 1a for schematic of the AJ printing system. Prior to printing, the substrates were cleaned with deionized water followed by isopropyl alcohol. The substrate surface was then cleaned using an atmospheric O_2 plasma (Atomflo™ 400, Surfx® Technologies LLC, Redondo Beach, CA) at 100 W power for 5 min to increase the surface hydrophilicity and adhesion with the printed film. The diameter of the nozzle used in this work was 150μ m. Note that the carrier gas flow rate controls the material flow while the sheath gas flow rate controls the mixing of the ink in the printhead and hence the 'sharpness' of the printed lines. The sheath gas and the carrier gas flow rates for the AJ system in this work were 50 +/- 5 sccm, and 25 +/- 5 sccm, respectively. The printing parameters, however, need to be optimized for different nanoparticle ink materials and manufacturers [30]. The lines were sintered at 400 °C for 30 min in a vacuum (10^{-2} – 10^{-3} Torr) furnace.

The method to measure the impedance of AJ printed lines is the same as that described in our previous work [11] but given here for completeness. Pyro-duct 597-A conductive epoxy (Aremco, Valley Cottage, NY) was used to connect the wires with the external circuit. Conductive epoxy was ambient cured over- night followed by heat cure at 93 °C for 2 h. A signal of 1 V and frequency in the range of 0.02–300 kHz was applied using a precision LCR meter (Agilent E4980A) with a 4-wire measurement. Before each measurement, a standard calibration method was performed to remove any parasitic effects. A programmable oven (Neytech Vulcan furnace, Model 3–550, Degussa-Ney Dental, Inc., Bloomfield CT) was used to heat the samples during the in-situ impedance measurements. Dwelling time for each temperature was 10 min, after which the impedance was measured.

An optical image of the representative printed and sintered Ni NP film (~7 mm long and ~ 545 μm wide) with probing pads is shown in Fig. 1b. A profilometer scan of the Ni NP film is shown in Fig. 1c. The thickness of the printed line was about 0.5 ± 0.1 μm. Considering the starting nanoparticle size of about 60 nm, we estimate that about 7–10 layers of the nanoparticles were deposited during the AJ process. A scanning electron micrograph of the sintered Ni film showing fused particles is given in Fig. 2d. The thickness of the line can be increased by the number of layers as was shown for AJ printed silver lines in our earlier work [6].

The impedance data for the Ni films at various frequencies and temperatures are shown in Fig. 2. The real part of film impedance, Z', at temperatures ranging from 25 °C to 500 °C at intervals of 50 °C for various frequencies is shown in Fig. 2a. Under ambient conditions, Z' increased about 0.2% between 20 Hz and 300 kHz. A monotonous increase in Z' was observed with an increase in the temperature up to about 350 °C. Fig. 2b shows the change in Z' as a function of temperature at different frequencies, while the temperature coefficient of resistance (TCR) values for various frequencies as a function of temperature are shown in Fig. 2c. Note that the TCR (/°C) is calculated as $\frac{R_2-R_1}{R_1\times(T_2-T_1)}$, where R_2 and R_1 are the resistance values at temperatures T_2 and T_1, respectively. In the range of 24 °C-350 °C TCR increased slowly as a function of temperature. It is well-known that the positive TCR for metals results from an increase in atomic vibrations that increase the electron scattering and hence resistance at higher temperatures. The frequency dependence of electrical conductivity is defined by the following equation [31],

$$\sigma(\omega) = \sigma(0)\left(\frac{1+i\omega\tau}{1+(\omega\tau)^2}\right), \quad (1)$$

where $\sigma(0)=\frac{ne^2\tau}{m}$, m is the effective mass of the electron, n is the number of electrons, τ is the collision time, ω is the frequency, and e is the charge on the electron. The conductivity thus decreases with frequency (at a given temperature) resulting in an increase in resistivity or Z'.

The measured TCR values for the sintered nanoparticle films ranged from ~ 0.0024/°C at 100 °C, to about ~ 0.0051/°C at 250 °C. These values are lower than the TCR value for bulk nickel, which is ~ 0.0059/°C at 20 °C. We note that the resistivity and TCR values for Ni films depend upon their gain size and thickness and are always reported to be lower than that for the bulk [32–35]. For example, the TCR for vacuum evaporated 70 nm thick Ni film was ~ 0.0023/°C [33], while another report [34] gives a values of 0.0008/°C at 50 °C and 0.0012/°C at 130 °C. Sputtered Ni films, 75 nm in thickness, were reported to have a TCR of about

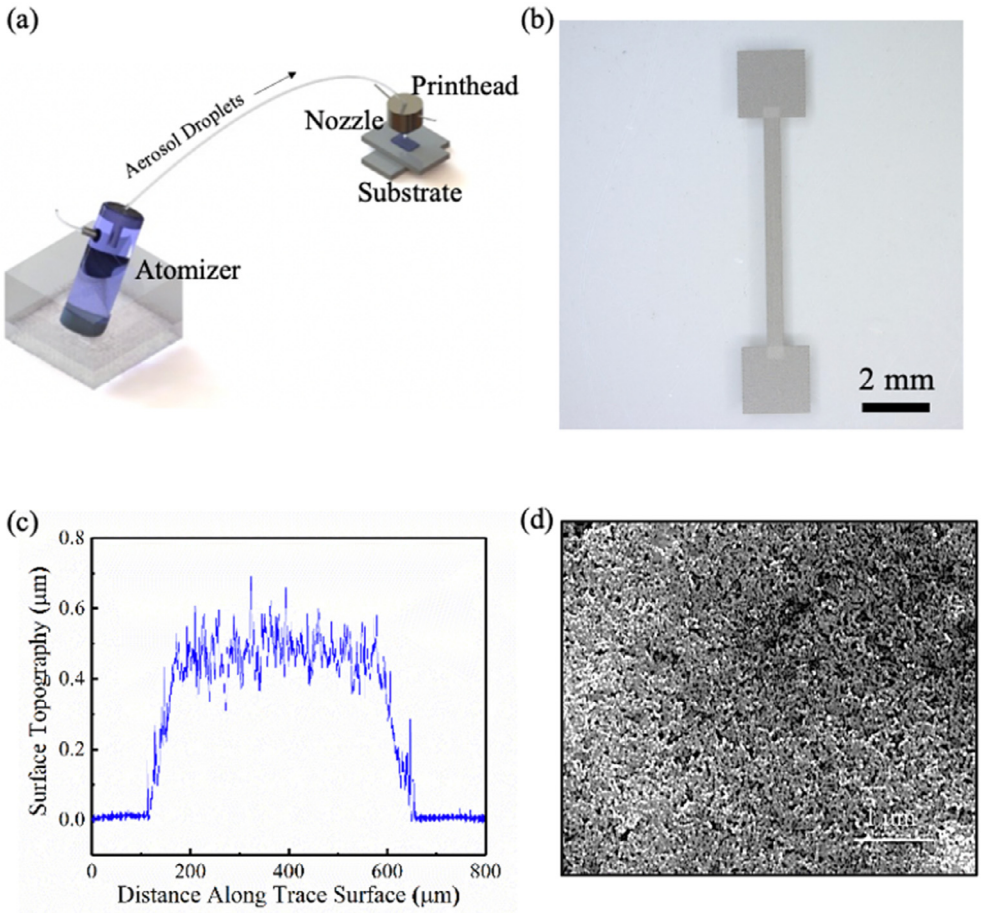

Fig. 1. (a) Schematic showing Aerosol Jet nanoparticle 3D printing apparatus consisting of an ultrasonic atomizer, a printhead, and a nozzle. (b) Optical imaging of the printed and sintered Ni film, (c) Profilometer scan of the printed element with an average height of approximately 500 nm, and (d) A scanning electron micrograph of the Ni film showing fused nanoparticles.

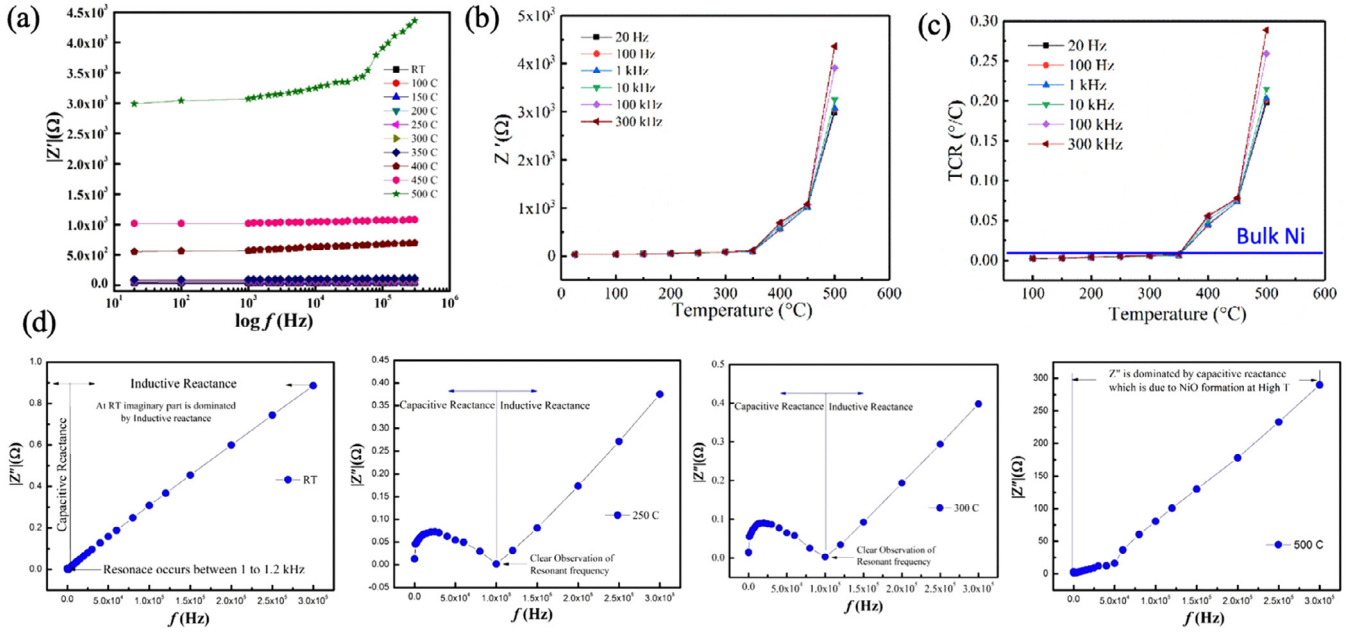

Fig. 2. Electrical behavior of Ni NP films at different temperatures (24 to 500 °C) and frequencies (0.02–300 kHz). A film sintering condition of 400 °C for 30 min in vacuum furnace was applied prior to the electrical measurements. a) The real part of impedance (Z') as a function of frequency measured at intervals of about 50 °C for different frequencies, b) real part of impedance (Z') as a function of temperature, c) TCR(/°C) as a function of temperature, and d) imaginary part of impedance (Z") as a function of different frequencies for room temperature, 250 °C, 300 °C, and 500 °C. The results show slight capacitive inductance (see Y-axis) at 250 °C and 350 °C, which increases by two orders of magnitude at 500 °C, indicating significant oxidation.

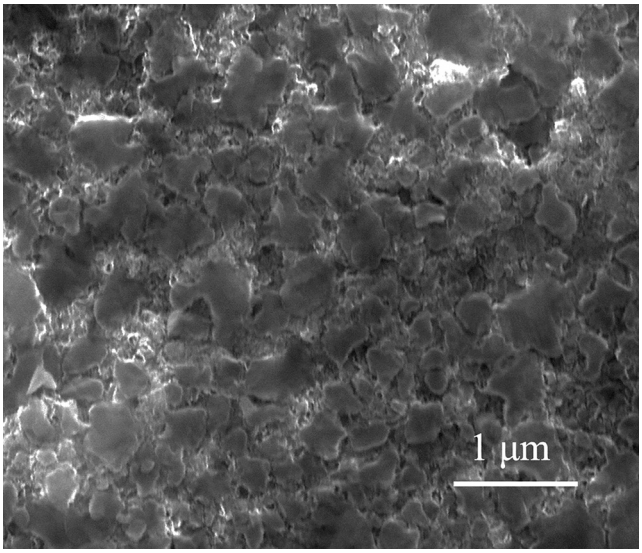

Fig. 3. SEM micrograph of the Ni film heated to 500 °C under ambient conditions during impedance measurements.

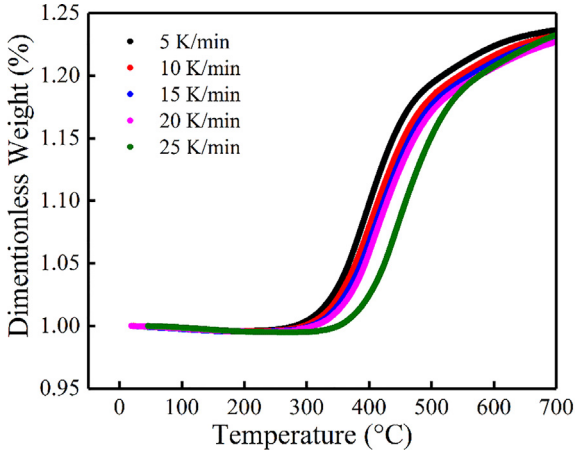

Fig. 4. TGA curves at different heating rates. TGA profiles show the start of gain in the weight beyond 300 °C for all heating rates and a similar profile for all the heating rates. The maximum weight gain for the samples is 23.28%.

0.003–0.005/°C at about 250 °C [35]. The observed TCR values from the current work (up to about 350 °C), are thus within the range of that expected from Ni films. This also indicates that the AJ printed films are primarily nickel metal, rather nickel oxide, up to 350 °C.

Upon further heating, however, the Z' for the films is seen to rapidly increase with increasing temperature. Fig. 2a and 2b show that Z' starts to increase by several orders of magnitude at temperatures beyond 350 °C, up to 500 °C, at all frequencies! The TCR increases from 0.0059 /°C at 350 °C to ~ 0.19773/°C (at 20 Hz) at 500 °C. The sudden changes in the slopes of Z' with temperature in Fig. 2b are indicative of the electrical instability, which is seen beyond 350 °C. The corresponding increase in the resistance of the film is represented in Fig. 2a and b. Note that in literature (Belser and Hicklin [35]), high values of TCR are ascribed to oxidation. The surface of the Ni film exposed to 500 °C under ambient conditions is shown in Fig. 3.

In order to understand the oxidation behavior of the films, we performed a TGA analysis of the nanoparticles used in this work (60 nm in size) and obtained the weight gain as a function of temperature from room temperature to 700 °C. The NPs in the current study were subjected to TGA analysis in a Discovery Series Thermogravimetric Analyzer (TA Instruments, New Castle, DE). The weight of the Ni NPs used for TGA was ~ 20.98 ± 0.92 mg. The Ni nanoparticles were placed on an Alumina pan and experiments were performed under atmospheric pressure conditions using air as the oxidant (same as that during operation of the films). The air flow rate was set at 10 ml min^{-1} for all the experiments. The experiments were started at room temperature and performed at five different heating rates varying from 5 to 25 K min^{-1} (both included) in steps of 5 K min^{-1}. Fig. 4 shows the dimensionless weight gain of Ni NPs as a function of temperature up to 700 °C.

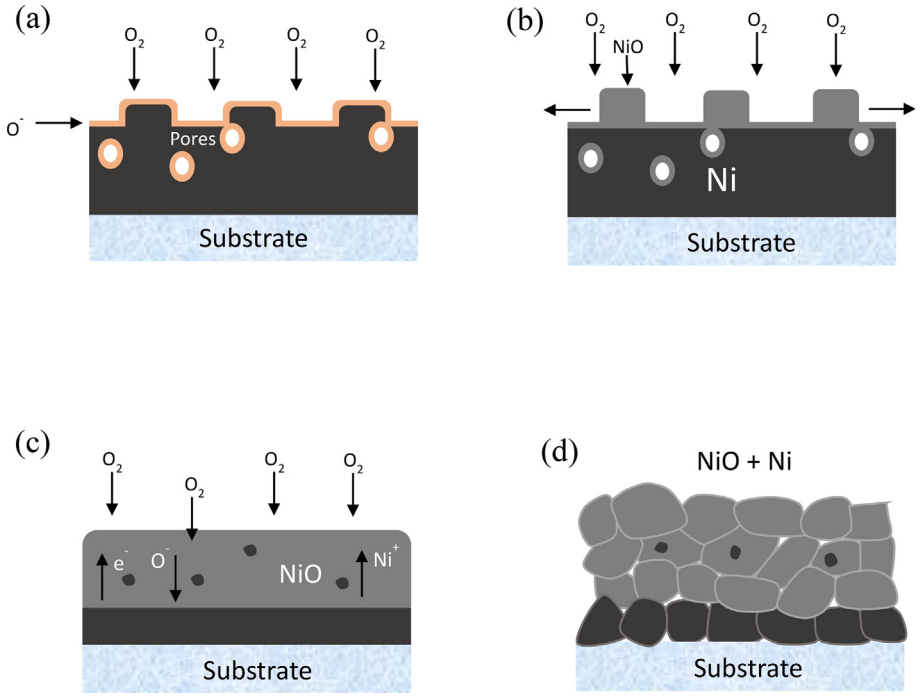

Fig. 5. Schematic of oxide layer formation in the AJ printed Ni film at high temperatures.

The TGA profiles show that the weight gain starts at about 325 °C for all the heating rates and that they exhibit very similar shapes. The maximum weight gain for the samples is 19.35% at 500 °C. The TGA results show that the weight gain at 700 °C is 23.7% and has not reached a maxima. However, literature shows that the maximum weight gain of Ni NPs is about 25.4% at 1000 °C [26]. Thus, at 500 °C with ~ 19.35% weight gain, the nanoparticles are at their near-saturation point (and heavily oxidized) which can partly explain the two order of magnitude increase in TCR at 500 °C (Fig. 2). Note that Ni nanoparticles with an average size of 28 nm started to oxidize at about 200 °C [26], which is lower than that observed in Fig. 4. However, the average nanoparticle size in their study [26] was only 50% of that in the current work, which can partly explain the difference in the temperature at which oxidation starts.

We speculate that the surface texture of the AJ-printed and sintered Ni films may initiate oxidation due to their high surface-to-volume ratios (Fig. 1c) and cause electrical instability. A schematic of the possible transport mechanisms involved during thermal oxidation for a AJ printed Ni thin film are shown in Fig. 5. The oxidation reaction in Ni film happens through an electron transfer at the interfaces, resulting in the formation of a monolayer of adsorbed O^- at the surface along with the diffusion of oxygen anions into the Ni film (Fig. 5a). The adsorbed O^- anions initially form small NiO islands[26] on Ni thin film surface as shown in Fig. 5(b). These oxide islands can grow as the temperature increases. Beyond 350 °C, growth of the oxide film may occur by both diffusion of O^- anions and Ni^+ cations at the Ni/NiO interface leading to heavy oxide layer formation as shown by Fig. 5c. As a result, TCR increases by greater than one order or magnitude as seen in Fig. 2c. Finally, at 500 °C, thermal oxidation affects the total morphology of the printed films and the oxidation reaches near saturation leading to a significant increase in the TCR as shown in Fig. 2c.

In summary, we show that AJ nanoparticle printing can be used to synthesize functional Ni films for high temperature applications, albeit with a lower maximum operating temperature (350 °C) than bulk nickel (600 °C). Further, we show that impedance characterization of the films at different frequencies and temperatures can capture their electrical stability at high temperatures. The 3D printed nickel films are electrically stable at all frequencies up to 350 °C but show an accelerated degradation beyond this temperature due to thermal oxidation. The onset of electrical instability is manifested in the impedance spectroscopy measurements as an increase in TCR by more than an order of magnitude. Possible mechanisms of oxidation of the film are discussed. Future studies will involve carefully changing the processing parameters to extend the thermal stability regime of the films beyond 350 °C and increase their use-range. The results thus advance our understanding of the fascinating area of printed electronic devices and their applications at high temperatures.

Declaration of Competing Interest

The authors declare that they have no known competing financial interests or personal relationships that could have appeared to influence the work reported in this paper.

Acknowledgements

This work was partially supported by the US Department of Energy, National Energy Technology Laboratory (NETL), under grant # DE-FE0031770 and # DE-FE0026170. We would like to thank Kathryn Mireles for her help with the TGA measurements.

References

[1] Paul BK, Panat R, Mastrangelo C, Kim D, Johnson D. Manufacturing of smart goods: current state, future potential, and research recommendations. J Micro Nano-Manuf 2016;4(4):044001.
[2] Saleh MS, Hu C, Panat R. Three-dimensional microarchitected materials and devices using nanoparticle assembly by pointwise spatial printing. Sci Adv 2017;3(3):e1601986.
[3] Yang H, Rahman MT, Du D, Panat R, Lin Y. 3-D printed adjustable microelectrode arrays for electrochemical sensing and biosensing. Sens Actuators, B 2016;230:600–6.
[4] Ali MA, Hu C, Jahan S, Yuan B, Saleh MS, Ju E, et al. Sensing of COVID-19 antibodies in seconds via aerosol jet printed three dimensional electrodes. Adv Mater 2021;33:202006647.
[5] Rahman MT, Rahimi A, Gupta S, Panat R. Microscale additive manufacturing and modeling of interdigitated capacitive touch sensors. Sens Actuators, A 2016;248:94–103.
[6] Rahman MT, Renaud L, Heo D, Renn MJ, Panat R. Aerosol based direct-write micro-additive fabrication method for sub-mm 3D metal-dielectric structures. J Micromech Microeng 2015;25(10):107002.
[7] Rahman MT, Cheng C-Y, Karagoz B, Renn M, Schrandt M, Gellman A, et al. High performance flexible temperature sensors via nanoparticle printing. ACS Appl Nano Materials 2019;2(5):3280–91.
[8] Rahman MT, Moser R, Zbib HM, Ramana C, Panat R. 3-D printed high performance strain sensors for high temperature applications. J Appl Phys 2018;123(2):024501.
[9] J. Brenneman, D. Tansel, G. Fedder, R. Panat, 2021, Interfacial Delamination and Delamination Mechanism Maps for 3D Printed Flexible Electrical Interconnects, Extreme Mechanics Letters, In Press.
[10] Hong K, Kim SH, Mahajan A, Frisbie CD. Aerosol jet printed p- and n-type electrolyte-gated transistors with a variety of electrode materials: exploring practical routes to printed electronics. ACS Appl Mater Interfaces 2014;6 (21):18704–11.
[11] Rahman MT, McCloy J, Ramana C, Panat R. Structure, electrical characteristics, and high-temperature stability of aerosol jet printed silver nanoparticle films. J Appl Phys 2016;120(7):075305.
[12] Joo M, Lee B, Jeong S, Lee M. Laser sintering of Cu paste film printed on polyimide substrate. Appl Surf Sci 2011;258(1):521–4.
[13] Park S-H, Kim H-S. Flash light sintering of nickel nanoparticles for printed electronics. Thin Solid Films 2014;550:575–81.
[14] Danaei R, Varghese T, Ahmadzadeh M, McCloy J, Hollar C, Sadeq Saleh M, et al. Ultrafast fabrication of thermoelectric films by pulsed light sintering of colloidal nanoparticles on flexible and rigid substrates. Adv Eng Mater 2019;21 (1):1800800.
[15] E.J. Fichtel, A.D. McDaniel, High temperature strain gage technology for gas turbine engines, in: N.A.a.S. Administration (Ed.) NASA, West Palm Beach, FL, United States, 1994.
[16] Chu S, Majumdar A. Opportunities and challenges for a sustainable energy future. Nature 2012;488(7411):294–303.
[17] Wilson WC, Atkinson GM. Passive wireless sensor applications for NASA's extreme aeronautical environments. Sensors Journal, IEEE 2014;14 (11):3745–53.
[18] Espalin D, Muse DW, MacDonald E, Wicker RB. 3D Printing multifunctionality: structures with electronics. Int J Adv Manufact Technol 2014;72(5):963–78.
[19] Kamyshny A, Magdassi S. Conductive nanomaterials for printed electronics. Small 2014;10(17):3515–35.
[20] Rahman MT, Mireles K, Gomez Chavez JJ, Wo PC, Marcial J, Kessler M, et al. High temperature physical and chemical stability and oxidation reaction kinetics of Ni–Cr nanoparticles. J Phys Chem C 2017;121(7):4018–28.
[21] N.R. Raravikar, R. Panat, Nanolithographic method of manufacturing an embedded passive device for a microelectronic application, and microelectronic device containing same, in: U.S. PTO (Ed.) May 2014.
[22] Raravikar N, Panat R, Jadhav S. Tombstone initiation model for small form-factor surface mount passives. IEEE Trans Compon Packag Manuf Technol 2012;2(9):1486–91.
[23] Unutulmazsoy Y, Merkle R, Rastegar I, Maier J, Mannhart J. Research update: ionotronics for long-term data storage devices. APL Mater 2017;5(4):042302.
[24] Song S-H, Xiao P. An impedance spectroscopy study of oxide films formed during high temperature oxidation of an austenitic stainless steel. J Mater Sci 2003;38(3):499–506.
[25] Luo L, Zou L, Schreiber DK, Olszta MJ, Baer DR, Bruemmer SM, et al. In situ atomic scale visualization of surface kinetics driven dynamics of oxide growth on a Ni–Cr surface. Chem Commun 2016;52(16):3300–3.
[26] Song P, Wen D, Guo ZX, Korakianitis T. Oxidation investigation of nickel nanoparticles. PCCP 2008;10(33):5057–65.
[27] Karmhag R, Niklasson GA, Nygren M. Oxidation kinetics of small nickel particles. J Appl Phys 1999;85(2):1186–91.
[28] Karmhag R, Tesfamichael T, Wäckelgård E, Niklasson GA, Nygren M. Oxidation kinetics of nickel particles: comparison between free particles and particles in an oxide matrix. Sol Energy 2000;68(4):329–33.
[29] Kumari SV, Natarajan M, Vaidyan V, Koshy P. Surface oxidation of nickel thin films. J Mater Sci Lett 1992;11(11):761–2.
[30] Saleh MS, Hu C, Brenneman J, Al-Muntasar AM, Panat R. 3D printed three-dimensional metallic microlattices with controlled and tunable mechanical properties. Addit Manuf 2021;39:101856.

[31] C. Kittel, Introduction to Solid State Physics WileyNovember 11, 2004.
[32] Hirschhorn J. On the electrical resistivity of thin nickel films. J Phys Chem Solids 1962;23:1821–3.
[33] Angadi MA, Udachan LA. Electrical properties of thin nickel films. Thin Solid Films 1981;79(2):149–53.
[34] Ghosh C, Pal A. Electrical resistivity and galvanomagnetic properties of evaporated nickel films. J Appl Phys 1980;51(4):2281–5.
[35] Belser RB, Hicklin WH. Temperature coefficients of resistance of metallic films in the temperature range 25 to 600 C. J Appl Phys 1959;30 (3):313–22.